



COVID-19-associated pulmonary aspergillosis in immunocompetent patients: a virtual patient cohort study

Henrique A. L. Ribeiro¹ · Yogesh Scindia¹ · Borna Mehrad¹ · Reinhard Laubenbacher¹

Received: 17 July 2022 / Revised: 10 May 2023 / Accepted: 21 May 2023 /
Published online: 12 June 2023

© The Author(s), under exclusive licence to Springer-Verlag GmbH Germany, part of Springer Nature 2023

Abstract

The opportunistic fungus *Aspergillus fumigatus* infects the lungs of immunocompromised hosts, including patients undergoing chemotherapy or organ transplantation. More recently however, immunocompetent patients with severe SARS-CoV2 have been reported to be affected by COVID-19 Associated Pulmonary Aspergillosis (CAPA), in the absence of the conventional risk factors for invasive aspergillosis. This paper explores the hypothesis that contributing causes are the destruction of the lung epithelium permitting colonization by opportunistic pathogens. At the same time, the exhaustion of the immune system, characterized by cytokine storms, apoptosis, and depletion of leukocytes may hinder the response to *A. fumigatus* infection. The combination of these factors may explain the onset of invasive aspergillosis in immunocompetent patients. We used a previously published computational model of the innate immune response to infection with *Aspergillus fumigatus*. Variation of model parameters was used to create a virtual patient population. A simulation study of this virtual patient population to test potential causes for co-infection in immunocompetent patients. The two most important factors determining the likelihood of CAPA were the inherent virulence of the fungus and the effectiveness of the neutrophil population, as measured by granule half-life and ability to kill fungal cells. Varying these

Borna Mehrad and Reinhard Laubenbacher: co-last-authors.

✉ Reinhard Laubenbacher
reinhard.laubenbacher@medicine.ufl.edu

Henrique A. L. Ribeiro
henrique.deassis@medicine.ufl.edu

Yogesh Scindia
yogesh.scindia@medicine.ufl.edu

Borna Mehrad
borna.mehrad@medicine.ufl.edu

¹ Department of Medicine, Division of Pulmonary, Critical Care, and Sleep Medicine, University of Florida, Gainesville 32610, FL, USA

parameters across the virtual patient population generated a realistic distribution of CAPA phenotypes observed in the literature. Computational models are an effective tool for hypothesis generation. Varying model parameters can be used to create a virtual patient population for identifying candidate mechanisms for phenomena observed in actual patient populations.

Keywords COVID-19 · Invasive aspergillosis · Coinfection · Immunocompetent host · Computational model · Virtual patient population

Mathematics Subject Classification 92-10

1 Introduction

Aspergillus fumigatus is an opportunistic fungus that can infect the lungs of immunocompromised hosts, including, among others, patients undergoing chemotherapy or receiving an organ transplant, and patients affected by chronic granulomatous disease (Latge 1999; Pappas 2010). Neutrophils are essential to fighting the pathogen, and impaired neutrophil responses are a common predisposing factor to the infection. More recently, patients with severe SARS-CoV2 infection have reportedly been affected by COVID-19 Associated Pulmonary aspergillosis (CAPA). However, Lai and Yu (2021) found that the conventional risk factors for aspergillosis were not present in CAPA patients.

Mitaka et al. (2021) found that around 10% of COVID-19 patients in ICUs develop invasive aspergillosis, and the mortality rate for these patients is 54% compared with 24% of those without CAPA (Ergun et al. 2021). According to Lai and Yu (2021), patients with CAPA are predominantly male, with an average age of 73 ± 13 years, and 88% had diabetes, high blood pressure, kidney disease, chronic obstructive pulmonary disease (COPD), or heart disease. The fact that CAPA is associated with these comorbidities but not with the conventional risk factors for invasive aspergillosis requires the generation of new hypotheses to explain the susceptibility of these hosts to the infection.

Computational models have been used extensively in immunology to create and test hypotheses. In particular, agent-based models have proven effective for studying respiratory diseases. They are intuitive, rule-based models that make it easy to represent heterogeneous spatial environments and individual entities, such as immune cells or pathogens, and their generation does not require extensive modeling expertise. We published an agent-based model of the innate immune response to *Aspergillus fumigatus* within an alveolar duct that established that one of the critical parameters determining infection outcome is the distance within which macrophages can detect fungal spores (Oremland et al. 2016).

In Ribeiro et al. (2022), we published an agent-based model of the immune response to *Aspergillus fumigatus*. The model focuses on the role of iron sequestration by the host as part of the innate immune response. It was parametrized entirely with information from the literature rather than data fitting, and was extensively validated with both data from the literature and our own time course data from experiments using

a mouse model of the infection. We also showed that variation of parametrizations from this reference model could account for the variability across experiments. A first result we obtained using the model demonstrates that fungal strains engage different parts of the innate immune response depending on their level of virulence. This computational model is the main tool for the results reported here.

We hypothesize that in patients with severe COVID-19, the destruction of the lung epithelium facilitates colonization by opportunistic pathogens. At the same time, the exhaustion of the immune system characterized by cytokine storms, apoptosis, and depletion of leukocytes hinders its ability to kill the fungus, explaining the susceptibility of otherwise immunocompetent patients to aspergillosis. We use the computational model to test this hypothesis and to ask what set of parameters and conditions explain CAPA. To test our hypothesis, we created a virtual patient population by sampling the model parameter space, characterizing patients with dual infection and analyzing disease outcomes, with each choice of parameters representing one virtual patient.

2 Material and methods

2.1 Modeling

The simulation study in this paper uses a computational model of the co-infection that is a modification of our previously published model (Ribeiro et al. 2022) capturing key features of the innate immune response to a respiratory *Aspergillus fumigatus* infection in immunocompetent hosts, including the role of iron regulation, an important virulence factor. The model spans the intracellular, tissue-level, and organism scales. At the tissue level, an agent-based model simulates the immune response in a spatially homogeneous representation of a volume of lung tissue. The domain simulated ($6.4 \times 10^{-2} \mu L$) is enough to represent a piece of lung infected with a few conidia. Its components are depicted in Fig. 1. The original model of immune response to *Aspergillus fumigatus* had 76 parameters; here, we use a reduced version of that model with 27 parameters (Table 4) by eliminating the iron regulation component and aggregating some of the cytokines represented explicitly. We describe the model in detail below.

The 3-dimensional space is homogeneous with periodic boundary conditions; that is, a 3-dimensional torus. If a molecule or agent leaves the simulation space by crossing one boundary, it re-enters from another, similar to previous modeling in this context (e.g., Castiglione et al. 2007; Ribeiro et al. 2017). The rationale for periodic boundary conditions is that the simulation covers a small volume amid a large infected volume. Therefore, the concentration of molecules across all boundaries should be similar.

As in our published model, we have three types of host cells: type II epithelial cells, macrophages, and neutrophils. These cells are equipped with a simple intracellular model (Fig. 2) that determines their state at any given time. They receive signals in the form of cytokines or contact with *A. fumigatus* and move to one of three final states: Active (macrophages, epithelial cells, and neutrophils), TNF primed (macrophages and epithelial cells), or Inactive (macrophages only). Each state allows the cell to engage in certain activities, such as secreting specific cytokines. Table 3 shows the

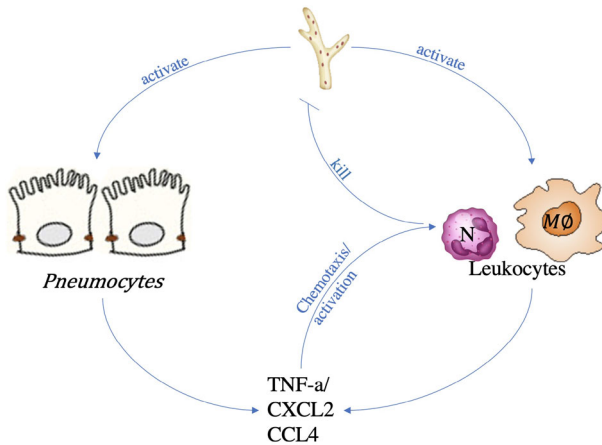


Fig. 1 Model description. *Aspergillus fumigatus* hyphae activate host cells (pneumocytes, monocytes, and neutrophils). Pneumocytes and monocytes secrete cytokines (TNF and IL-10) and chemokines (CXCL2 and CCL4). The chemokines chemoattract other leukocytes (neutrophils and monocytes) to the infection site, and the cytokines (TNF), together with the fungus itself, activate the leukocytes. Leukocytes kill *A. fumigatus*. This simplified figure does not show inactivation by IL-10/TGF- β /apoptotic cells and the secretion of TGF- β by inactivated cells

interactions between agents and molecules and the outcomes of these interactions. It is worth noting that only active macrophages can kill hyphae, while neutrophils in any state can kill. That was an assumption in our previous model, based on evidence that macrophages need pre-activation to kill hyphae (Roilides et al. 1995, 1994).

Figure 2 and Table 3 summarize most features of the model dynamics. As mentioned, in this model we do not include iron metabolism explicitly, thereby significantly reducing the number of parameters. We also assumed that there were no significant changes in cell counts over time, due to the fact that we only simulate a 24 h period, based on the observation in Gago et al. (2018) that the number of monocytes and neutrophils is approximately constant from day two to three, which makes our assumption reasonable. We used two minute time steps in order to correctly capture the dynamics of diffusion, since a longer time step would lead to near equilibrium in the diffused molecules.

Besides cells, the model also contains five molecules: IL10, TNF, TGF- β , CCL4, and CXCL2. These molecules diffuse through the space according to a partial differential equation (Chang et al. 1991) and interact with cells with probability given by Eq. 1:

$$p = 1 - e^{-x/k_d}, \quad (1)$$

where p is the probability that the receptor will be activated, x is the cytokine concentration, and k_d is its dissociation constant. This equation is also used for the reaction between granules and hyphae. In this case, x is the granule concentration in arbitrary units, k_d is $k_d_GRANULE$, and p is the probability that the hyphal septae will die. In the case of hyphae killing by granules this equation is a phenomenological approximation. Moreover, a given molecule's concentration decays with a half-life of one

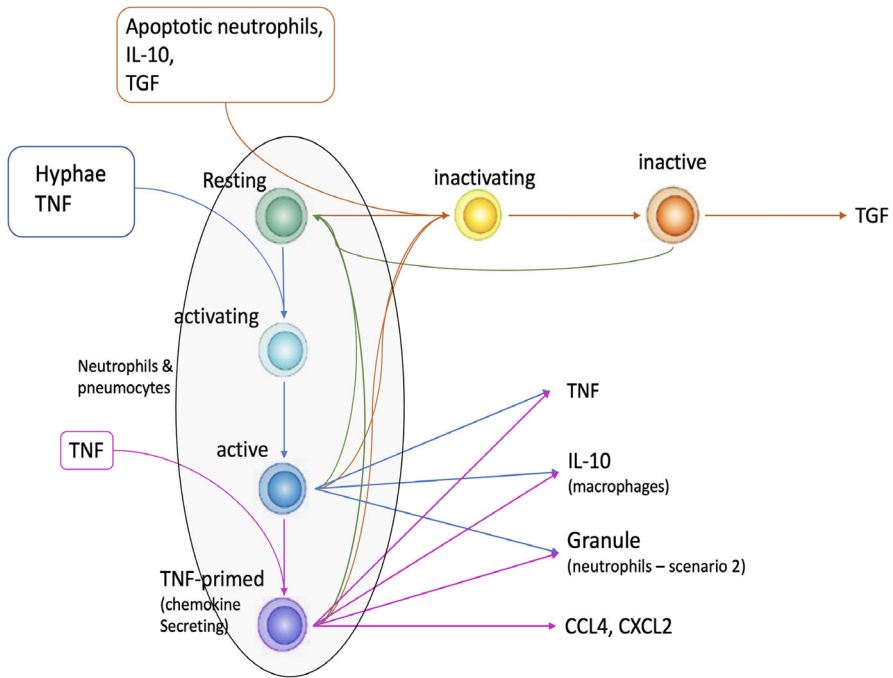


Fig. 2 Diagram showing host cell state changes. In response to TNF or hyphae, resting host cells move to the activating state, and after 60 iterations activating cells become active. Active cells extra primed with TNF become chemokine secreting. Macrophages primed with TGF- β , IL-10, or apoptotic cells become "inactivating" and then inactive (TGF- β secreting). After 180 iterations, inactive, active, or TNF-primed cells return to the resting state without extra signaling. The times to move from one state to another are approximations using the times for gene activation and inactivation measured in *in-vitro* experiments (Ribeiro et al. 2022)

hour and a continuous exchange with the serum (Eq. 2):

$$y = x * e^{-K_{turn}*t}, \tag{2}$$

where K_{turn} is the turnover rate, and t is the time-step size (2 min).

The two mechanisms not covered so far are leukocyte movement and *A. fumigatus* growth. Like in our published model, in the absence of chemokines, cells move randomly, while in their presence, they tend to move to the voxels with higher chemokine concentrations. The rate of movement is constant, and the cells will, on average, traverse a fixed number of voxels per time step. In the presence of chemokines, each voxel receives a weight according to Eq. 3, where CCL4 guides macrophages and CXCL2 guides neutrophils (Ribeiro et al. 2022):

$$w_i = 1 - e^{-y_i/k_d}, \tag{3}$$

where w_i is the weight of the i -th neighbor voxel, y_i is the chemokine concentration in the i -th voxel, and k_d is the dissociation constant.

In nature, hyphal growth is of course a continuous process composed of elongation and branching (chiefly sub-apical branching). In the model we represent hyphal growth and branching as a discrete approximation. Every 40 μm of septae was considered a unit (we called it a cell in the simulator). A tip cell can produce another tip cell (elongation), while a sub-tip cell can form a 45° branch (subapical branch) (Maheshwari 2005; Riquelme and Bartnicki-Garcia 2004) with a 25% probability. Other cells cannot originate new cells unless their neighbors are killed and they become tip or sub-tip cells again. In this paper, we did not change the branching probability, and to vary the growth rate, we changed the time it takes for a tip cell to generate a new unit.

2.2 Modeling coinfection

We model the COVID-19 *A. fumigatus* coinfection implicitly by changing specific parameters as well as the number of leukocytes in the lung space (Table 1). In the model, neutrophils kill hyphae by direct contact. However, to accommodate alternative mechanisms of neutrophil anti-microbial function, we introduced a second scenario in which leukocytes secrete granules that diffuse and kill the fungus. In our published model, we considered neutrophils killing *A. fumigatus* via ROS secretion only. The ROS concentration to kill hyphae is high enough only in the synapsis between the neutrophil and hyphae. However, other granule molecules may also be able to kill hyphae, hence the second scenario to account for uncertainty in the mechanism.

The results for the second scenario are presented in the supplementary material. For the second scenario, we introduced the parameters (k_d _GRANULE and GRANULE_HALF_LIFE—Table 5). Upon interaction with *A. fumigatus*, neutrophils are activated and then secrete one arbitrary unit of granule (an abstraction for the molecules contained in neutrophil granules). This granule kills hyphae with a probability given by Eq. 1. The granule contents, like all molecules, decay with a given half-life (GRANULE_HALF_LIFE). The rationale for using arbitrary units is that all that is needed is a pair of values, GRANULE_QTTY and k_d _GRANULE, that fits the data in Ribeiro et al. (2022). This pair of parameters is not identifiable, so we fixed GRANULE_QTTY to one arbitrary unity and fit the k_d to reproduce the simulation data in our previous work.

In Ribeiro et al. (2022), iron sequestration acted to inhibit *Aspergillus fumigatus* growth. Here we do not consider the role of iron explicitly. Instead, we tested a wide range of hyphal growth rates (Table 1) to represent more or less permissive lung environments, partly as the result of variable availability of nutrients such as iron across the space (see below). Another contributing factor is the damage done to the epithelium by the ongoing viral infection.

In this study, we focus on five parameters, with values listed in Table 1. The first parameter is the intrinsic growth rate of the fungus. The second and third parameters are proxies for the strength of the immune response, and the fourth and fifth parameters reflect an increased number of immune cells as part of the response to the viral infection. The intrinsic growth rate of the hyphae encapsulates the permissivity of the environment, such as the nutrient availability. However, the collective effects of the

intrinsic growth rate, together with the counteracting effects of the immune response, we call the observed growth rate.

We performed Latin-Hypercube Sampling (LHS) on the parameters in Table 1. We varied the number of leukocytes, the monocyte killing probability (the probability with which monocytes kill hyphae upon direct contact), the intrinsic growth rate, and the neutrophil killing probability (the probability with which neutrophils kill hyphae upon direct contact). The intrinsic growth rate varies between 2.75 and 80 $\mu\text{m}/\text{h}$. The rationale for these values is that the host limits access of the fungus to nutrients, thereby decreasing its growth rate. Therefore, at the lowest restriction, the fungus will grow to its full potential. The literature measure *A. fumigatus* growth in vitro of 40 $\mu\text{m}/\text{h}$ (see our previous work Ribeiro et al. (2022)) and 60 $\mu\text{m}/\text{h}$ Gago et al. (2018). Because there is uncertainty in these numbers and in-vitro growth may be conservative, we set the maximum to 80 $\mu\text{m}/\text{h}$.

The probability of neutrophils and macrophages killing hyphae had a similar rationale. We had the default from our previous work of 23% and 9.9%, respectively. Because we are considering the negative effect of SARS-CoV-2 in these cells (See Results and Discussion), these numbers can only decrease. Meanwhile, the number of leukocytes reflects the uncertainty and natural variability in these cells. We use the ranges given by Gago et al. (2018) (5–15 million) as an educated guess. Note that at the peak, on day one, we have 15 million neutrophils, and on day three, 15 million monocytes. Therefore, these ranges are reasonable for both cell types.

Using LHS sampling we generated 24,000 parameter sets, representing 24,000 virtual hosts of the dual infection. (We also created an additional 36,000 virtual hosts using the alternative neutrophil mechanism; see supplementary material). We measured the observed growth rate as the slope of the log of the *A. fumigatus* curve across the 24 h of simulation (Eq. 4). Note that we shifted the *A. fumigatus* curve by 1 to avoid negative infinity when the number of *A. fumigatus* cells tends to zero. The observed growth rate is a value given by Eq. 4, while the intrinsic growth rate is a model parameter (Table 1). In Eq. 4 we are counting the number of hyphal septae:

$$\text{Log}_{10}(\text{hyphae} + 1) = a + b \times t, \quad (4)$$

where b is the observed growth rate, and t is time in hours.

2.3 Partial rank correlation coefficient

A partial rank correlation coefficient is a common way to assess local model sensitivity to parameters. In this paper, we performed a sensitivity analysis (SA) of the five (Scenario 1) and six (Scenario 2) parameters against *A. fumigatus* observed growth rate. We used the method “pcc” from the R package “verification” (Johnson and Lebreton 2004). To do the SA we used our virtual patient population.

Moreover, we also measured how the parameters’ partial correlation changed as the intrinsic growth rate changed. That is, we divided the virtual patient population into ten bins of similar intrinsic growth rates (GROWTH_RATE). Then we computed

Table 1 Model parameter ranges

Parameter	Description	Parameter range	Reference value	References
GROWTH_RATE	intrinsic growth rate	2.75–80 $\mu\text{m}/\text{h}$	40 $\mu\text{m}/\text{h}$	Ribeiro et al. (2022)
PR_N_KILL	probability of neutrophils to kill hyphae	0.23–23%	23%	Ribeiro et al. (2022)
PR_MA_KILL	probability of monocytes to kill hyphae	0.099–9.9%	9.9%	Ribeiro et al. (2022)
NUM_MA	number of monocytes	360–960 cells	960 cells	Gong et al. (2011)
NUM_N	number of neutrophils	360–960 cells	360	Gong et al. (2011)

The table shows the ranges in which we sample parameters (maximum and minimum value). Column 1: parameter name; Column 2: description; Column 3: parameter range; Column 4: parameter reference value; Column 5: rationale for the value in Column 4. The values taken from Ribeiro et al. (2022) are the default values in our previous work

the partial rank correlation coefficient of the other four parameters (PR_N_KILL, PR_MA_KILL, NUM_MA, and NUM_N).

2.4 Code

The simulator was written in Java (JavaSE–1.8) and needs only the JRE System Libraries. A typical execution takes about 4–5 s to simulate 24 h in an OSX 2.6 GHz 6-Core Intel Core i7. Code is available at: <https://github.com/deassisinfo/CAPA/>.

3 Results

Our goal is to test the hypothesis that a respiratory viral infection such as severe COVID-19 can make the lung environment more permissive to *A. fumigatus* growth and, at the same time, exhaust the immune system, allowing the fungal infection to progress in an otherwise immunocompetent host. In the simulator, these conditions translate into a higher intrinsic growth rate and lower ability of leukocytes to kill hyphae. Concomitantly, when the *A. fumigatus* infection starts, the number of leukocytes in the lung is high because the host is already fighting another infection. These conditions are encoded by the model parameters in Table 1. Each parameter sample can be thought of as a virtual patient for whom we simulate infection outcome. We started each simulation with 640 type-II pneumocytes, 20 germinated conidia, and 360–960 monocytes and neutrophils. Each simulation represented 24 h (720 iterations), and we used a time-step of 2 min. The results are shown in Fig. 3.

In order to correctly interpret Fig. 3, one needs to keep in mind the distinction between intrinsic growth rate and observed growth rate. The first is a parameter (Table 1) that controls the time it takes for new *A. fumigatus* cells to be generated. The second results from the number of cells generated (intrinsic growth rate) minus the number of cells killed by leukocytes. The intrinsic growth rate is always positive, while the observed growth rate may be negative if the infection is declining, as observed in the vast majority of cases in Fig. 3.

Observe that the distinction between intrinsic and observed growth rates is exclusively a model property. The intrinsic growth rate is a model parameter, whereas the observed rate is a model output. However, from the point of view of nature or a more complex model, what we call intrinsic may still be considered observed. For example, a simple model may have a growth rate with a value of 3 $\mu\text{m}/\text{h}$. Therefore, for this model, 3 $\mu\text{m}/\text{h}$ is its intrinsic growth rate. However, a more complex model may have two parameters: growth rate and iron acquisition, none of which are 3 $\mu\text{m}/\text{h}$. But they interact to produce an observed growth rate of 3 $\mu\text{m}/\text{h}$.

The data in Fig. 3 show a prominent peak in negative observed growth rate, indicating resolution of the infection, and a second smaller peak with a long tail of positive observed growth rate. We can therefore cluster patients into two groups, with Cluster 1 containing only patients that clear the infection. Cluster 2 can be further subdivided into three subclusters representing progressively worsening fungal infection. Cluster 2A is the portion of Cluster 2 with negative observed growth rate, representing

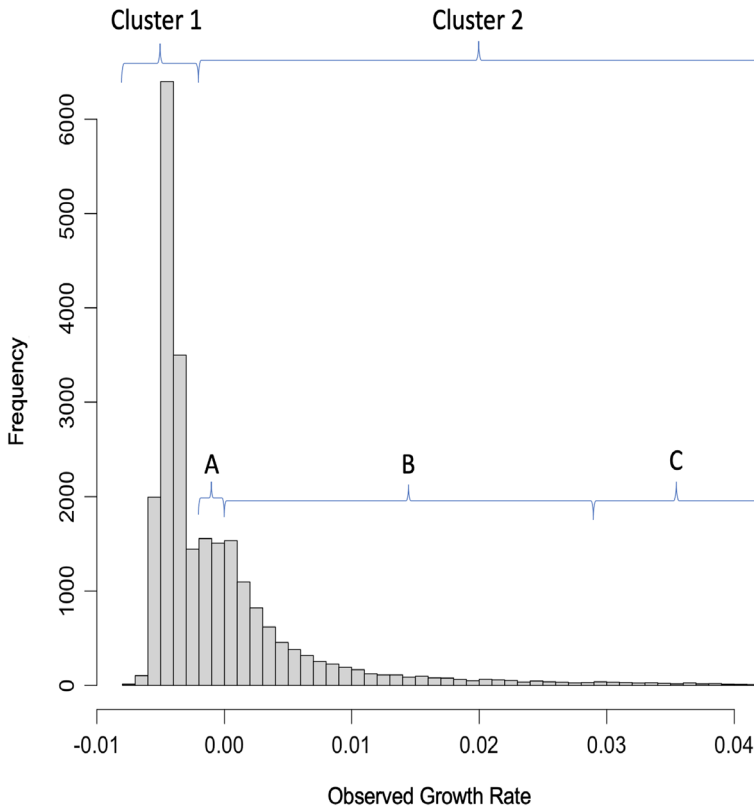


Fig. 3 Distribution of observed growth rate. The observed growth rate of *A. fumigatus* was measured during the 24 h of simulation in the virtual patient population. The graph shows a bimodal distribution of the growth rate. We divided the virtual patients into two clusters according to their observed growth rate: the prominent peak on the negative side (Cluster 1) and the secondary peak (Cluster 2). We then subdivided Cluster 2 into three subclusters: 2A is the negative part, 2B is the positive part excluding outliers, and 2C is the long tail of outliers

patients whose infection clears, while Cluster 2B is the portion of Cluster 2 with positive observed growth rate (excluding the outliers), and Cluster 2C is the long tail of outliers (Fig. 3), both together representing patients that develop CAPA. We found a similar distribution in Scenario 2 (Fig. 8). This bimodal distribution is consistent with what is known for this disease: patients with an intact neutrophil response resolve the fungal infection, whereas the cluster with positive observed growth rate corresponds to the observation that COVID-19 patients in the ICU can develop CAPA (Mitaka et al. 2021). Figure 7 shows that the percentage of patients with CAPA in our simulation (clusters 2B and 2C) is similar to the one measured in epidemiological studies.

Clusters 2B and 2C in Fig. 3 and Table 6 suggest that a combination of higher intrinsic fungal growth rate and lower fungal killing by the immune response can explain the onset of CAPA in otherwise immunocompetent hosts. Figure 10 confirms that patients with CAPA have decreased ROS production by neutrophils, one of the key tools used by leukocytes to kill hyphae. This reduction is qualitatively similar to the reduction in

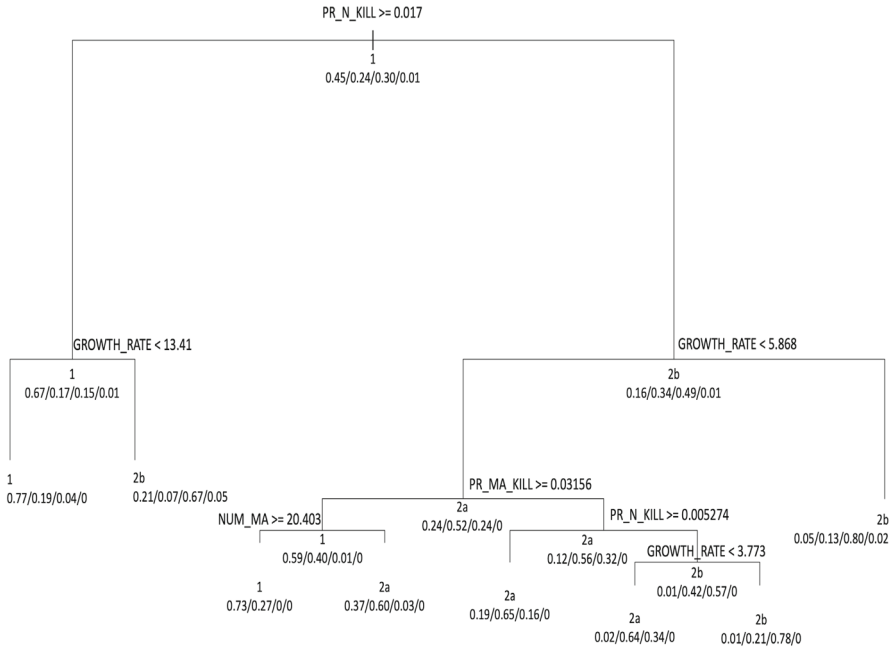


Fig. 4 Classification tree. The classification tree found the parameter values that best parse the virtual patients into the four clusters defined in Fig. 3. The percentage value range is 0–1. The sets of four numbers beneath each branch are the relative frequencies of each cluster in that branch

neutrophil-killing ability between CAPA and non-CAPA patients (Fig. 10B). Meanwhile, Fig. 11 shows that hemorrhage and the availability of heme is a factor that favors *A. fumigatus* growth, similar to the increase in the observed growth rate observed in our CAPA virtual patients (Fig. 11C). Interestingly in Scenario 2, the intrinsic growth rate seems to play a secondary role (Table 2). To further explore this hypothesis, we constructed classification trees to see which combinations of parameters are necessary for CAPA (Fig. 4).

One can see in Fig. 4 that the dominant parameters are the neutrophil killing rate, intrinsic growth rate, and to a lesser degree, the monocyte killing rate. Classification trees can indicate which parameters are the most important by measuring how much each parameter contributes to node purity. We confirmed that these three parameters (neutrophil killing rate, intrinsic growth rate, and monocyte killing rate) are indeed the dominant ones. Similarly, in Scenario 2, granule half-life, k_d , and to a lesser degree, intrinsic growth rate are the dominant parameters (not shown, Fig. 9).

Since we have only three dominant parameters, we can plot the virtual patients in a 3D space. That will allow us to see how the four clusters are distributed. In Fig. 5A, each point represents a virtual patient. The x-axis is the log of that patient’s intrinsic growth rate, the y-axis is the log of that patient’s monocyte killing probability, and the z-axis is the log of that patient’s neutrophil killing probability. We colored each patient according to their cluster (1, 2A, 2B, or 2C). We used log base ten because different patients have parameter value differences of up to two orders of magnitude.

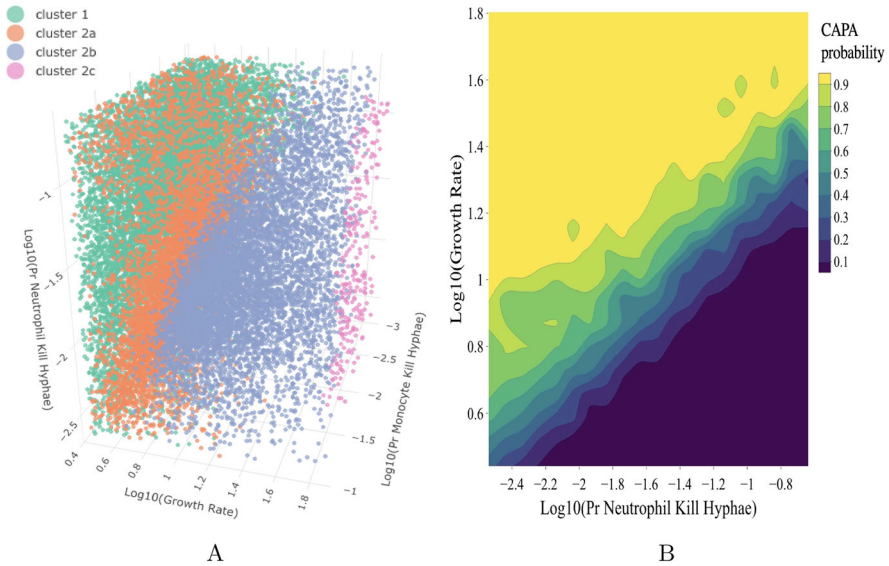


Fig. 5 Distribution of clusters of patients and CAPA probability in the 3D and 2D spaces formed by the most important parameters according to the classification tree (Fig. 4). **A** virtual patients plotted in 3D space and colored according to their cluster. The x-axis is the log of patients' intrinsic growth rate, the y-axis is the log of their monocyte killing probability, and the z-axis is the log of the neutrophil killing probability. **B** shows the CAPA probability as the intrinsic growth rate and neutrophil killing probability

As shown in Fig. 5A, Clusters 1 and 2A are interspersed. This is to be expected because both these clusters represent patients for whom the infection cleared (Cluster 2A is the negative part of peak 2). Cluster 2C is segregated in the high intrinsic growth rate region. However, it is noteworthy that some patients in Cluster 2B are very similar to patients in Cluster 2A, in that they have similar sets of parameters that characterize their infection.

To better explore this transition between patients that clear the infection (Clusters 1 and 2A) and those that do not (Clusters 2B and 2C), we computed how the probability of developing CAPA changes as parameters vary (Fig. 5B). We restrict ourselves to plotting the CAPA probability across the two most influential parameters. We plot how a virtual patient's probability of developing CAPA changes as the intrinsic growth rate and the neutrophil killing rate change (Fig. 5B). As shown in Fig. 5B, the dividing line along which a patient may either clear the infection or develop CAPA cuts the graph across the diagonal. Both parameters (intrinsic growth rate and neutrophil killing probability) are essential in determining the patient's outcome: a high intrinsic growth rate can be compensated for, in part, by a high killing rate and vice versa. In Scenario 2, we found a similar transition between patients that develop CAPA and those that do not when we vary the parameters of intrinsic growth rate and granule k_d (Fig. 9B). This shows that our conclusions are similar in both scenarios.

An essential question in Fig. 5, especially 5B, is whether using only two parameters is meaningful. To answer that question, we divided the virtual patients into two subsets. The first subset of 20,000 was used to train classification trees, while the second

Table 2 The predictive power of parameters

Parameters	F1-cross-validation	F1-test
ALL	0.7379	0.7430
Top-three	0.7380	0.7393
Top-two	0.7108	0.7163

The predictive power of classification trees was evaluated in cross-validation and test sets when these trees were trained using all five parameters, the top three parameters (GROW_RATE, PR_N_KILL, and PR_MA_KILL), or the top two (GROW_RATE and PR_N_KILL). Column 1 parameters used in the model; Column two F1 score in cross-validation; Column 3 F1 score in the test set

subset of 4000 was used to test its predictive power. We also used ten-fold cross-validation and measured the F1 score, as in Table 2. The F1 score combines the precision and recall into a single metric, and it is primarily used to compare the performance of a classifier. We found that the reduction from all five parameters to the top three (GROW_RATE, PR_N_KILL, and PR_MA_KILL) does not affect the predictive power of the classification trees, while the reduction to the top two (GROW_RATE and PR_N_KILL) has only a minor effect.

Results from previous figures have shown that the observed growth rate is highly dependent on the intrinsic growth rate. We divided the virtual population into ten bins of similar intrinsic growth rates and computed the square of the partial rank correlation of the parameters and observed growth rate (Fig. 6). Figure 6A shows the variation of the square of the correlation between neutrophil killing probability and observed growth rate. At the same time, Fig. 6B shows the variation of the square of the correlation between monocyte killing probability and observed growth rate. The partial correlation between the other parameters and the observed growth rate was not substantial (results not shown).

4 Discussion

Aspergillus fumigatus is an opportunistic mold that infects immunocompromised hosts, chiefly those with impaired neutrophil response, but also patients with normal neutrophils but impaired cell-mediated immunity (Mackel and Steele 2019). However, Lai and Yu (2021) found that in patients with CAPA the conventional risk factors for invasive aspergillosis are not present. They found that CAPA patients were mostly older men suffering from diabetes, obesity, hypertension, or cardiovascular disease. These conditions may help explain the onset of CAPA, but are likely not sufficient by themselves. We hypothesized that COVID-19 infection may exhaust the immune system, and at the same time the destruction of lung epithelium overloads the fungus with nutrients. Therefore we propose a model where the coinfection negatively affects the default parameters we inherited from Ribeiro et al. (2022). We tested this hypothesis using a simulated virtual patient population generated by our computational model.

Before we can draw conclusions from the model, it is critical to discuss the parameters. Like our previous one, this model was parameterized with literature data.

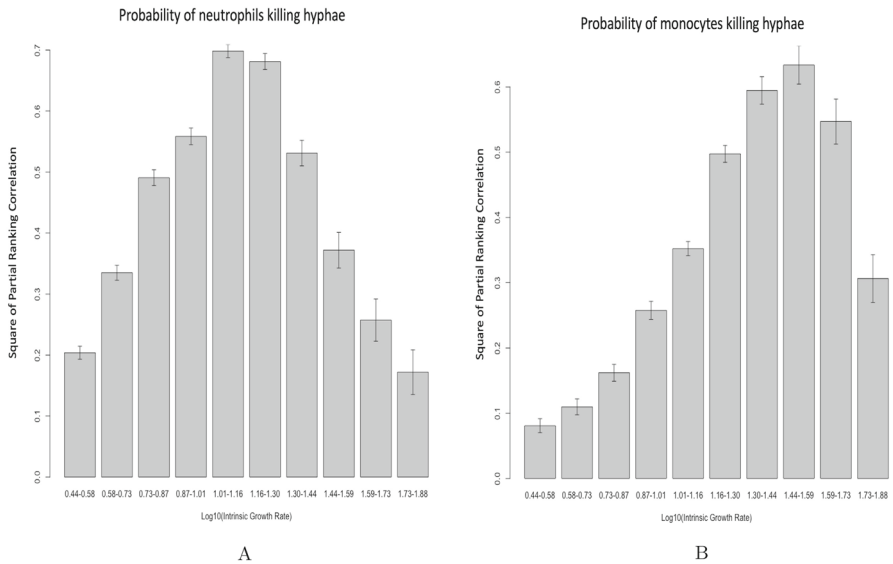


Fig. 6 Variation of the square of the correlation r^2 between the critical model parameters and the observed growth rate, with the variation of the intrinsic growth rate. We started with a dataset of 24,000 virtual patients generated with LHS and then partitioned this dataset by intrinsic growth rate. The x-axis shows the range of the intrinsic growth rate in each partition. We then calculate the correlation between parameters and the observed growth rate in each partition. **A** Variation of r^2 between the neutrophil killing rate and observed growth rate. **B** Variation of r^2 between monocyte killing rate and observed growth rate. Error bars are standard deviations calculated with bootstrap

Therefore it does not fit any particular dataset exactly. However, it reproduces biological data within the limit of biological variance itself. That was the case with the several datasets with which we compared our model in our previous paper (Ribeiro et al. 2022). We note that it is possible, to fit this model to particular data sets.

Another point that is worth discussing is identifiability. Because of the way parameters were obtained from the literature (see Ribeiro et al. 2022), identifiability is not an issue here. As an example, take cytokines k_d , secretion rate, and half-life. If one tries to fit these parameters from a time series of cytokines in BAL or lung homogenate in an infection, likely, they will not be identifiable. However, we got these parameters from experiments designed to measure each one individually.

Concerning the experiments we conducted, our simulations show that 31% of the virtual patients in Scenario 1 and 17% in Scenario 2, who were exposed to *A. fumigatus*, developed CAPA. That is qualitatively consistent with data from Mitaka et al. (2021) that show 10% of patients in the ICU developed CAPA and with data from Kariyawasam et al. (2021) that show that 15% of patients in the ICU developed CAPA (Fig. 7). Moreover, Figs. 10 and 11 suggest that the kinds of parameter variations proposed in this model (i.e., change in *A. fumigatus* virulence and neutrophil activity) exist in the general population. On the other hand, the discrepancy, chiefly in Scenario 1, can be explained by the fact that most patients hospitalized with COVID-19 infection are presumably not exposed to *A. fumigatus*.

Results from Fig. 7 show that Scenario 2 seems to agree more with epidemiological data, but it also shows a discrepancy between the two scenarios. This highlights the fundamentally different dynamics of neutrophils killing by direct contact or secreting granules that kill hyphae in the neighborhood. Both scenarios were made to fit the simulations in Ribeiro et al. (2022). However, the two scenarios diverged when we varied the conditions, albeit still behaving in similar ways.

Our model suggests that both reducing neutrophil activity and increasing fungal intrinsic growth rate might be necessary for CAPA to emerge (Figs. 4 and 5). Tappe et al. (2022) found that neutrophils of COVID-19 patients had reduced ROS production qualitatively similar to the reduction in neutrophils' killing ability in simulated CAPA patients in our model (Fig. 10). At the same time, Grunwell et al. (2019) found that neutrophils treated with airway supernatant of patients with acute respiratory failure due to lower respiratory tract viral infection had altered surface markers. Moreover, when the neutrophils were treated with airway supernatant in patients with bacterial and viral coinfection, they had decreased respiratory burst and bactericidal response. The mechanism is not well understood. However, Verweij et al. (2020) reported that influenza might suppress neutrophil oxidative burst, causing temporary disease status resembling chronic granulomatous disease. Arastehfar et al. (2020) indicate that collateral effects of antiviral immunity may, paradoxically, contribute to an inflammatory environment that favors secondary infections such as CAPA. On the other hand, the drugs used to treat serious COVID-19 infection, such as Tocilizumab and dexamethasone, can also hinder the immune response against *A. fumigatus* (Segrelles-Calvo et al. 2021). These findings support the hypothesis that the immune response against *A. fumigatus* may be hampered in patients with serious COVID-19 infection.

Concomitantly, Escobar et al. (2015) showed that pneumocytes cocultured with *A. fumigatus* inhibited fungal germination and growth. In contrast, Rodrigues et al. (2005) found that exposing *A. fumigatus* to albumin increases its germination and growth rate. Hsu et al. (2018) gives a persuasive argument for hemorrhaging increasing the rate of *A. fumigatus* invasion. Likewise, Michels et al. (2022) found that heme increases fungal growth (Fig. 11). While Fig. 11B shows only the effect of heme *in-vivo* Michels's paper (Michels et al. 2022) gives compelling evidence that heme iron and perhaps heme ring favors *A. fumigatus* growth *in-vitro* and *in-vivo*.

In our previous model, iron concentration was a bottleneck reducing the observed growth rate (Ribeiro et al. 2022). Hemorrhage caused by previous COVID-19 infection may help to overcome this bottleneck, according to the evidence provided by (Hsu et al. 2018; Michels et al. 2022). Furthermore, the iron concentration (non-heme) may be higher in serum than in the alveolar space (Stites et al. 1995). Arastehfar et al. (2020) argue that the leading risk factor for CAPA includes severe lung damage during the course of COVID-19 and the presence of comorbidities such as structural lung defects. These findings support our hypothesis that lung epithelium destruction and hemorrhage favor *A. fumigatus* growth: once the pneumocytes are killed, *A. fumigatus* is exposed to a nutrient-rich environment and can grow faster.

Figure 5 suggests that the onset of CAPA is regulated chiefly by the intrinsic fungal growth and neutrophil killing rates. The CAPA probability increases as the intrinsic growth rate increases or as the neutrophil killing probability decreases. In the alternative neutrophil action scenario (Fig. 9), we can make a similar observation with the

granule K_d and intrinsic growth rate (Fig. 9B). A moderate increase in the intrinsic growth rate and decrease in neutrophil activity can also lead to CAPA. Alternatively, a high increase in intrinsic growth rate or a steep decrease in neutrophil activity could also lead to the same outcome. Both scenarios we tested (i.e., neutrophils killing by direct contact or by secreting granules) support this conclusion. We found the first hypothesis to be more plausible (i.e., moderate change). However, Grunwell, JR et al. 2018 Grunwell et al. (2019) found a substantial reduction in neutrophil killing ability that could support the second hypothesis (i.e., high change in neutrophil killing probability). Whether their result generalizes to fungal coinfection remains open.

Figure 6 shows that neutrophils are more efficient in controlling the infection in the case of a moderate intrinsic growth rate. This corroborates the previous results. It may also reflect how identifiable these two parameters are. Figure 6 can be divided into two: the center and the tails. In the tails, the leukocytes always win or lose the battle independent of the value of the intrinsic growth rate. But that means that the observed growth rate in these regions is not strongly correlated with leukocyte activity. The center is where there is an exchange: as the intrinsic growth rate increases, the neutrophil and monocyte activity has to increase to keep the fungus in check. That means that these two parameters are not identifiable from the point of view of the observed growth rate. That reinforces the previous conclusion that CAPA may be caused by decreased leukocyte activity, increased *Aspergillus fumigatus* growth, or both.

Figures 5B and 9B, however, suggests that CAPA might be caused by both instead of only one of the causes. The tails and the center in Fig. 6 roughly relate to the plateaus and the dividing line in Figs. 5B and 9B. Note that there are only narrow areas of intrinsic growth rate that are entirely independent of neutrophil activity. That is, the dividing line in graphs 5B and 9B cuts the plot along the diagonal.

Interestingly, the work of Dellière et al. (2021) analyzed several clinical factors in COVID-19 patients with and without CAPA. Treatment of COVID-19 patients with the antibiotic azithromycin was associated with an increased risk of CAPA. In prior literature, azithromycin has been shown to attenuate neutrophil oxidative burst (Čulić et al. 2002). In our model, this would translate into a decreased neutrophil-killing probability. This fits with our finding that this parameter is paramount for CAPA establishment.

On the other hand, Dellière et al. (2021) found similar percentages of neutrophils and macrophages in CAPA and non-CAPA patients. Likewise, Xu et al. (2021) found that patients with fewer than 1.5×10^9 neutrophils/L had no increased risk of developing CAPA. That resonates with our finding that the number of neutrophils and monocytes had a low correlation with the observed growth rate (Table 6) and was a poor predictor of CAPA (Figure trees) (Fig. 4).

The work we present here is primarily theoretical, validated with supporting evidence from the literature. While it would be very difficult to validate our predictions using actual patient data, one could instead use data from experiments with mouse models of aspergillosis and COVID-19. Such an experiment would involve three groups of mice: non-neutropenic ACE2 transgenic mice challenged with *Aspergillus*, ACE2 mice challenged with SARS-CoV2, and SARS-COV2 followed by *Aspergillus*. One could then use data on fungal load and cytokine measurements after 3 days.

We conclude that an increase in the favorability of the lung environment, likely due to an increased supply of nutrients and decreased effectivity of neutrophils to kill hyphae, is the most likely explanation for CAPA. To make our findings more robust, we tested two possible scenarios of how neutrophils kill hyphae (Supplementary Material). We found that the conclusions are the same, independent of the scenario.

Author Contributions The study was conceived and carried out by HALR, with scientific input from the other authors. RL and BM provided funding for the project and contributed to the writing of the manuscript.

Funding This work was partially supported by NIH Grants DE021989, EB024501, AI135128, and AI117397; and NSF Grant CBET-1750183.

Data availability Simulation data available on request.

Declarations

Conflict of interest The authors do not have any conflicts of interest or competing interests.

Ethics approval The manuscript complies with the ethical standards of the Journal for Mathematical Biology.

Consent to participate Not applicable.

Consent for publication All authors have approved the manuscript.

Code availability Code available upon request.

Appendix A Supplementary Material

A.1 Rules

Table 3 shows the rules used in the model, all taken from Ribeiro et al. (2022). That is, the rules in this model are a subset of the rules in our previous model. The reduction in the number of rules is related to the fact that we are not simulating iron explicitly. Second, we start the model with already germinated conidia (i.e., small hyphae). Therefore, rules such as the interaction of leukocytes with conidia and conidia germination are unnecessary. Table 4 shows the parameters in the model; again, all taken from Ribeiro et al. (2022), except for the number of leukocytes. Subsequently, we provide a brief rationale for all the parameters with references.

A.2 Parameters

The k_d of TNF, IL10, TGF, CCL4, and CXCL2. The k_d values from these molecule receptors are reported by Samson et al. (1997), Sai et al. (2004), Al-Alwan et al. (2013), Liu et al. (1994), Tan et al. (1993), Ho et al. (1993), Carson et al. (1995), Schall et al. (1990), Aggarwal et al. (1985), Tsujimoto et al. (1985), Baglioni et al. (1985), Tsujimoto and vilcek (1987), Stauber et al. (1988), Hohmann et al. (1989),

Table 3 Table depicting the rules of how agents and field variables interact

Interaction	Description	Type	Outcome
Macrophage-neutrophil	Macrophage phagocytose apoptotic neutrophil	Probabilistic: constant probability	Inactivating signal: macrophage change to inactivating or remains inactive
Macrophage-Aspergillus	Active Macrophage kills hyphae	Probabilistic: constant probability	Activating signal: macrophage remains active; hyphae gets killed
Macrophage-IL10	Active or inactive Macrophage secrete IL10	Deterministic: fixed amount	Local IL10 concentration increases
Macrophage-TGF-b	Inactive Macrophage secrete TGF-b	Deterministic: fixed amount	Local TGF-b concentration increases
Macrophage-TNF	Active macrophage secrete TNF	Deterministic: fixed amount	Local TNF concentration increases
Macrophage-CCL4	TNF-primed Macrophage secrete CCL4	Deterministic: fixed amount	Local CCL4 concentration increases
Macrophage-CXCL2	TNF-primed Macrophage secrete CXCL2	Deterministic: fixed amount	Local CXCL2 concentration increases
Macrophage-IL10	Macrophage is primed by IL10	Probabilistic: probability computed by Eq. 1	Inactivation signal: macrophage change to inactivating or remains inactive
Macrophage-TGF-b	Macrophage is primed by TGF-b	Probabilistic: probability computed by Eq. 1	Inactivation signal: macrophage change to inactivating or remains inactive
Macrophage-TNF	Macrophage is primed by TNF	Probabilistic: probability computed by Eq. 1	Activating signal: macrophage change to activating; if it is active it transitions to TNF-primed and starts to secrete chemokines
Neutrophils-Aspergillus	Neutrophils kills hyphae	Probabilistic: constant probability	Activating signal: neutrophils change to activating or remains active; hyphae is killed

Table 3 continued

Interaction	Description	Type	Outcome
Neutrophil-granule	Neutrophil secrete granule	Deterministic: fixed amount	Local concentration of granule increases
Pneumocyte-Aspergillus	Pneumocyte interacts with germinating conidia or hyphae	Probabilistic: fixed probability	Activating signal: pneumocyte change to activating or remains active
Pneumocyte-TNF	Active pneumocyte secrete TNF	Deterministic: fixed amount	Local concentration of TNF increases
Pneumocyte-CCL4	TNF-primed pneumocyte secrete CCL4	Deterministic: fixed amount	Local concentration of CCL4 increases
Pneumocyte-CXCL2	TNF-primed pneumocyte secrete CXCL2	Deterministic: fixed amount	Local concentration of CXCL2 increases
Pneumocyte- TNF	Pneumocyte is primed by TNF	Probabilistic: probability computed by Eq. 1	Activating signal: pneumocyte change to activating; if it is active it transitions to TNF-primed and starts to secrete chemokines
Granule-Aspergillus	Granule kill hyphae	Probabilistic: probability computed by Eq. 1	Hypphae is killed (Scenario 2 only)

The first column shows the two entities involved in the interaction. The second column briefly describes the interaction; the third indicates whether it is deterministic or probabilistic and how the probability is computed. The fourth column describes the outcome of the interaction in case of success. Note that two entities (Column 1) can interact in more than one way

Ding et al. (1989), Massague and Like (1985), Kalter and Brody (1991), Wakefield et al. (1987). In cases where we have more than one value we used the median.

The TNF, IL10, TGF, CCL4, CXCL2 secreting rates come from Werner et al. (2009), Taylor et al. (2007, 2014), Gersuk et al. (2006), Hohl et al. (2005), Chai et al. (2010), Celio et al. (2006), Fadok et al. (1998), Steele et al. (2005), Adachi et al. (1994), Okazaki et al. (1995), Brummer et al. (2003), Mihai et al. (2003), Marika et al. (2002), Warris et al. (2005), Fadok et al. (2001), Fujishima et al. (1993), Xing and Remick (2003), Altstaedt et al. (1996), Bondeson et al. (1999), Abe et al. (1999), Loeffler et al. (2009), Simitsopoulou et al. (2007), Lord et al. (1991), Cassatella (1995), Ciesielski et al. (2002), Palmberg et al. (1998), Jablonski et al. (2016), Katsuo and Bo-Ram (2014), Thorley et al. (2007). For more detail see Ribeiro et al. (2022).

Diffusion rate of cytokines is reported by Goodhill (1997, 1998).

Half-life of cytokines is reported by Huhn et al. (1997), Zahn and (1989), Oliver et al. (1993), Kuribayashi (2018), Castell et al. (1988), Toft et al. (2011), Wakefield et al. (1990).

This movement rate can be obtained from Khandoga et al. (2009). The value, 1.44 $\mu\text{m}/\text{min}$, is conservative compared to other sources. Pollmächer and Figge (2014) uses a movement rate of 2–6.4 $\mu\text{m}/\text{min}$, for instance. Nevertheless, the rate used here must be considered a phenomenological movement rate. In the real lung, leukocytes may not move in a straight line but along the alveolar curved surface. That is the case in the Pollmächer and Figge (2014) model.

Growth rates come from papers that report hyphal length over time (Bocking et al. 1999; Escobar et al. 2015; Gago et al. 2018; Meletiadiis et al. 2001), while branching probability was based on the hyphal growth unit length. This gives an estimate of how many branches per septum there are Trinci (1973), Bocking et al. (1999).

Monocyte and neutrophil killing probabilities are extrapolated from the killing rate of in vitro experiments from Zarembor et al. (2007), Gazendam et al. (2016a, b), Roilides et al. (1998, 1995, 1994)). Likewise for the pneumocyte interaction rate (Wakefield et al. 1990). For more details see Ribeiro et al. (2022).

Turnover rate comes from the difference between lung and serum IL-6 concentration (Goncalves et al. 2017). For more details see Ribeiro et al. (2022).

Monocyte and neutrophil half-life is reported in Patel et al. (2017); Tak et al. (2013).

Septae length is reported in Ding et al. 2015; Renshaw et al. 2018.

The time that cells need to change status (T_{CHANGE} and T_{REST} - Fig. 2) were based on in vitro reports (Sharif et al. 2017).

Number of macrophages and monocytes comes from mice infected with influenza (Gago et al. 2018). While the number of pneumocytes comes from Dzhuraev et al. (2019) (Table 5).

A.3 Model Equations

Here, we add some additional information on the equations and parameters in the model. We calculate the molecule's half-life by decreasing their amount by a specific percentage each iteration in each voxel, which is equivalent to Euler's approximation

Table 4 Parameters used in the model

Parameter	Description	Value	References
TNF_QTTY	TNF secretion quantity	$1.46 \times 10^{-20} \text{ mol} \times \text{cell}^{-1} \times \text{h}^{-1}$	Ribeiro et al. (2022)
IL10_QTTY	IL-10 secretion quantity	$6.97 \times 10^{-22} \text{ mol} \times \text{cell}^{-1} \times \text{h}^{-1}$	Ribeiro et al. (2022)
TGF_QTTY	TGF- β secretion quantity	$1.01 \times 10^{-21} \text{ mol} \times \text{cell}^{-1} \times \text{h}^{-1}$	Ribeiro et al. (2022)
CCL4_QTTY	CCL4 secretion quantity	$1.79 \times 10^{-20} \text{ mol} \times \text{cell}^{-1} \times \text{h}^{-1}$	Ribeiro et al. (2022)
CXCL2_QTTY	CXCL2 secretion quantity	$1.11 \times 10^{-19} \text{ mol} \times \text{cell}^{-1} \times \text{h}^{-1}$	Ribeiro et al. (2022)
k_d _TNF	k_d TNF receptor	326 pM	Ribeiro et al. (2022)
k_d _IL10	k_d IL10 receptor	140 pM	Ribeiro et al. (2022)
k_d _TGF	k_d TGF- β receptor	26.5 pM	Ribeiro et al. (2022)
k_d _CCL4	k_d CCL4 receptor	180 pM	Ribeiro et al. (2022)
k_d _CXCL2	k_d CXCL2 receptor	91.667 pM	Ribeiro et al. (2022)
D	Diffusion coefficient	$850 \mu\text{m}^2/\text{min}$	Ribeiro et al. (2022)
r	Elongation rate	$40 \mu\text{m}/\text{h}$	Ribeiro et al. (2022)
PR_BRANCH	Branch probability	25%	Ribeiro et al. (2022)
MV_RATE	Leukocyte move rate	$1.44 \mu\text{m}/\text{min}$	Ribeiro et al. (2022)
N_H_KILL	Probability of neutrophil killing hyphae	22.71%	Ribeiro et al. (2022)
MA_H_KILL	Probability of macrophage killing hyphae	9.81%	Ribeiro et al. (2022)
E_INT	Epithelial cells-Aspergillus interaction rate	4.49%	Ribeiro et al. (2022)
L	Molecule half-life	1 h	Ribeiro et al. (2022)
TURNOVER_RATE	Molecule exchange rate between lung and whole body serum	0.1823 h^{-1}	Ribeiro et al. (2022)
MA_HALF_LIFE	Macrophage half-life	24 h	Ribeiro et al. (2022)
N_HALF_LIFE	Neutrophils-half-life	6 h	Ribeiro et al. (2022)
SEPTAE_L	Septa length	$40 \mu\text{m}$	Ribeiro et al. (2022)
ITER_CH_STATE	Iterations for cell to change state	60	Ribeiro et al. (2022)
ITER_TO_REST	Iterations for cell to return to resting state	180	Ribeiro et al. (2022)
NUM_MA	Number of macrophages	960	Gago et al. (2018)
NUM_N	Number of neutrophils	360	Gago et al. (2018)
NUM_P	Number of pneumocytes	640	Ribeiro et al. (2022)

The first column gives the parameter name; the second a short description; the third the parameter value; and the fourth a bibliographic reference. Note that apart from the number of leukocytes, all parameters were inherited from our previous model

Table 5 Model parameter ranges for the alternative scenario. The table shows the ranges in which we sample parameters (maximum and minimum value)

Parameter	Description	Parameter range	Reference value	References
GROWTH_RATE	Intrinsic growth rate	2.75–80 $\mu\text{m/h}$	40 $\mu\text{m/h}$	Ribeiro et al. (2022)
PR_MA_KILL	Probability of monocytes to kill hyphae	0.099–9.9%	9.9%	Ribeiro et al. (2022)
K_d _GRANULE	K_d of the reaction between granule and hyphae	1×10^8 – 1×10^{10}	1×10^{10}	Ribeiro et al. (2022)
GRANULE_HALF_LIFE	Granule half-life	0.033–3.33h	0.67h	Ribeiro et al. (2022)
NUM_MA	Number of monocytes	360–960 cells	960 cells	Gong et al. (2011)
NUM_N	Number of neutrophils	360–960 cells	360	Gong et al. (2011)

Column 1: parameter name; Column 2: description; Column 3: parameter range; Column 4: parameter reference value; Column 5: rationale for the values in Column 4. The values taken from Ribeiro et al. (2022) are the default values in our previous work. The values for GROWTH_RATE, PR_MA_KILL, NUM_MA, and NUM_N are the same as in Table 1

Table 6 Table with the sensitivity analysis (SA) of the parameters used to create the virtual population

Parameter	Scenario-1	Scenario-2
GROWTH_RATE	0.5538 ± 0.0050	-0.0317 ± 0.0061
PR_N_KILL	-0.5497 ± 0.0042	NA
PR_MA_KILL	-0.3170 ± 0.0061	-0.0788 ± 0.0052
NUM_N	-0.1114 ± 0.0062	-0.1093 ± 0.0050
NUM_MA	-0.0780 ± 0.0064	-0.0535 ± 0.0050
GRANULE_HALF_LIFE	NA	0.5929 ± 0.0038
<i>K_d</i> _GRANULE	NA	-0.3809 ± 0.0049

The parameter range is shown in Table 5. First column parameters description; Column 2 partial rank correlation for Scenario 1; Column 3 partial rank correlation for Scenario 2

of the solution of the following differential equation:

$$\frac{dx}{dt} = -k * x \tag{A1}$$

where *k* is not equal to but can be calculated from the parameter *L* in Table 4. To compute *k* from the parameter *L* in the table, we have to notice that the above equation has the solution:

$$x(t) = x_0 * e^{-k*t} \tag{A2}$$

where $x(L)/x_0 = 0.5$; therefore, $k = -\ln(0.5)/L$

Notice that molecules also decay as an effect of turnover with the serum (Eq. 2). Similarly, the leukocytes (Macrophages and Neutrophils) die every iteration with fixed probability which approximates the above differential equation.

Molecules diffuse through the space with the partial differential equation:

$$\frac{\partial S}{\partial t} = D * \nabla^2 S \tag{A3}$$

where *D* is the diffusion coefficient (Table 4), we solve this equation using an implicit method with periodic boundary conditions.

A.4 Supplementary Results

This supplementary material contains results from Scenario 2, sensitivity analysis, and comparisons of simulated results with the literature (Table 6 and Figs. 7, 8, 9, 10, 11).

Fig. 7 Comparison between epidemiological data on CAPA (Kariyawasam et al. 2021) and virtual epidemiology. ICU patients and intubated patients refer to epidemiological data from Kariyawasam et al. (2021). Scenarios 1 and 2 are simulation data. Error bars represent standard deviation

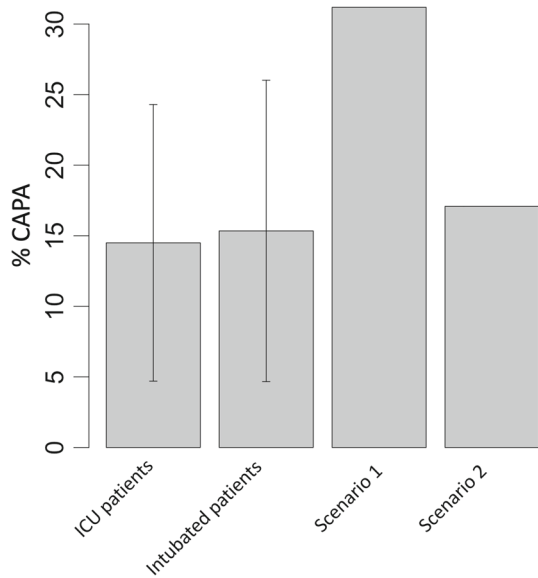
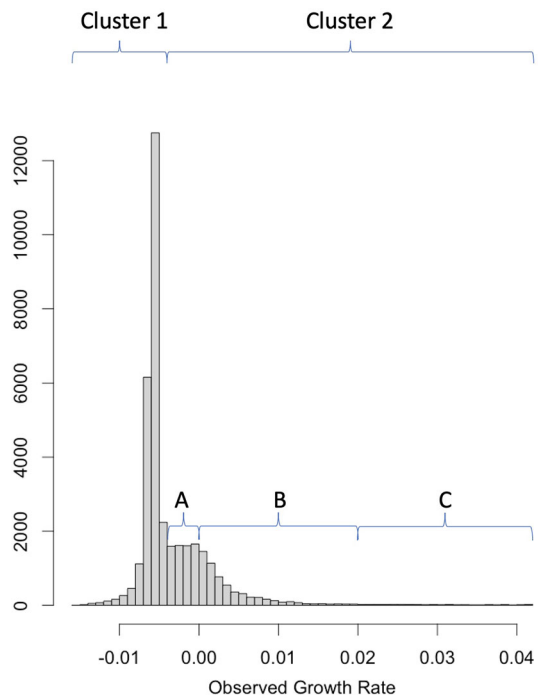


Fig. 8 Distribution of observed growth rate in the alternative scenario where neutrophils do not need direct contact to kill hyphae. We divided virtual patients into two clusters: the prominent peak on the negative side (Cluster 1) and the secondary peak (Cluster 2). We then subdivided Cluster 2 into three subclusters: 2A is the negative part, 2B is the positive part excluding outliers, and 2C is the long tail of outliers



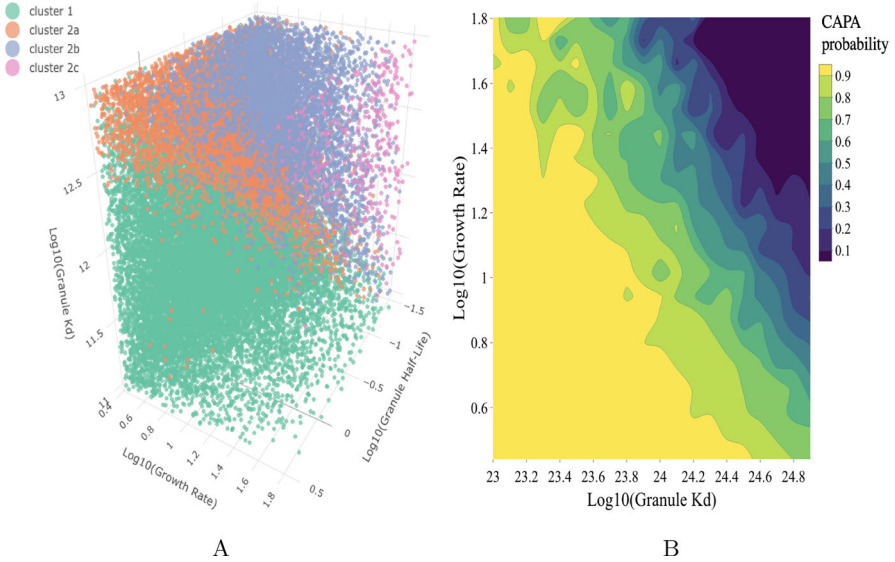


Fig. 9 Plots in 3D space of the most important parameters according to the classification tree (not shown) in the alternative scenario where neutrophils do not need direct contact to kill hyphae. **A** Virtual patients plotted in 3D space. The x-axis is the log of patients’ intrinsic growth rate, the y-axis is the log of their neutrophil granule k_d , and the z-axis is the log of the neutrophil granule half-life. **B** shows the CAPA probability as the intrinsic growth rate and neutrophil granule k_d change

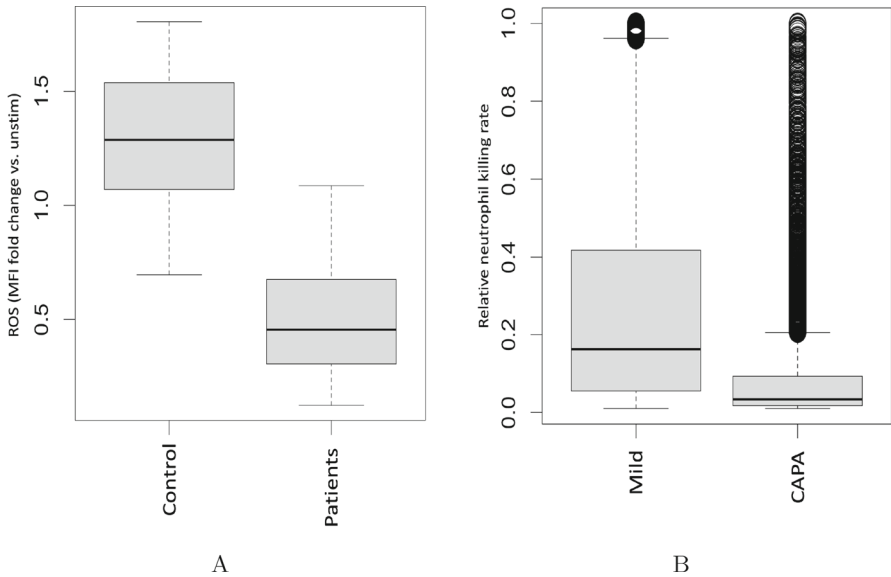


Fig. 10 Immune system inhibition by SARS-CoV-2. **A** decrease in ROS production in patients with SARS-CoV-2 (Tappe et al. 2022). **B** decrease in neutrophil killing ability in virtual patients with CAPA relative to patients without CAPA (Scenario 1)

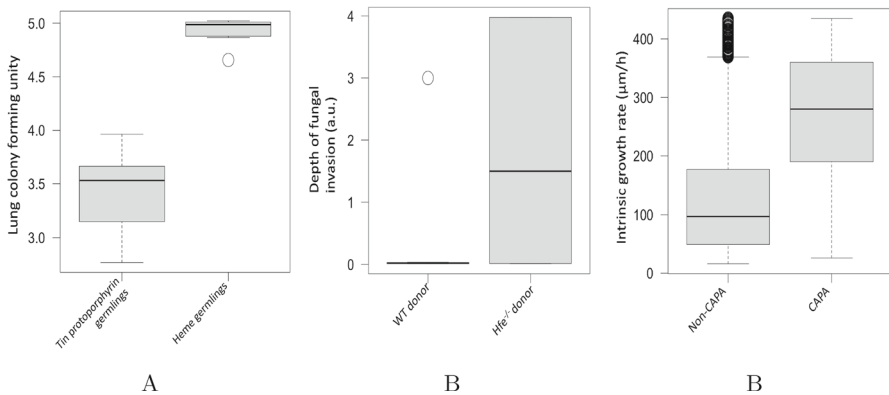


Fig. 11 Hemorrhage leads to increased *A. fumigatus* growth *in-vivo* due to iron availability. **A** Mice treated with heme and infected with *A. fumigatus* had more lung colony-forming units than litter mates treated with Tin protoporphyrin. **B** Lung transplant causes micro-hemorrhage that predisposes mice to fungal invasion due to iron availability. Hemochromatosis mice *Hfe*^{-/-} mice had more fungal invasion control when infected with *A. fumigatus* after receiving a lung transplant. **C** simulated CAPA virtual patients (Scenario 1) had higher intrinsic growth rates, similar to what A and B suggest for mice with hemorrhage

References

- Abe Y, Hashimoto S, Horie T (1999) Curcumin inhibition of inflammatory cytokine production by human peripheral blood monocytes and alveolar macrophages. *Pharmacol Res* 39(1):41–7. <https://doi.org/10.1006/phrs.1998.0404>
- Adachi Y, Okazaki M, Ohno N, Yadomae T (1994) Enhancement of cytokine production by macrophages stimulated with (1 → 3)-beta-d-glucan, grifolan (grn), isolated from *Grifola frondosa*. *Biol Pharm Bull* 17(12):1554–1560. <https://doi.org/10.1248/bpb.17.1554>
- Aggarwal B, Eessalu T, Hass P (1985) Characterization of receptors for human tumour necrosis factor and their regulation by γ -interferon. *Nature* 318:665–667. <https://doi.org/10.1038/318665a0>
- Al-Alwan LA, Chang Y, Mogas A, Halayko AJ, Baglole CJ, Martin JG, Rousseau S, Eidelman DH, Hamid Q (2013) Differential roles of cxcl2 and cxcl3 and their receptors in regulating normal and asthmatic airway smooth muscle cell migration. *J Immunol* 191(5):2731–2741. <https://doi.org/10.4049/jimmunol.1203421>
- Altstaedt J, Kirchner H, Rink L (1996) Cytokine production of neutrophils is limited to interleukin-8. *Immunology* 89:563–568. <https://doi.org/10.1046/j.1365-2567.1996.d01-784.x>
- Arastehfar A, Carvalho A, van de Veerdonk FL, Jenks JD, Koehler P, Krause R, Cornely OA, Perlin DS, Lass-Flörl C, Hoenigl M (2020) Covid-19 associated pulmonary aspergillosis (capa)-from immunology to treatment. *J Fungi*. <https://doi.org/10.3390/jof6020091>
- Baglioni C, McCandless S, Tavernier J, Fiers W (1985) Binding of human tumor necrosis factor to high affinity receptors on hela and lymphoblastoid cells sensitive to growth inhibition. *J Biol Chem* 260(25):13395–7
- Bocking SP, Wiebe MG, Robson GD, Hansen K, Christiansen LH, Trinci APJ (1999) Effect of branch frequency in *Aspergillus oryzae* on protein secretion and culture viscosity. *Biotechnol Bioeng* 65:638–648. [https://doi.org/10.1002/\(SICI\)1097-0290\(19991220\)65:6<638::AID-BIT4>3.0.CO;2-K](https://doi.org/10.1002/(SICI)1097-0290(19991220)65:6<638::AID-BIT4>3.0.CO;2-K)
- Bondeson J, Browne K, Brennan F, Foxwell B, Feldmann M (1999) Selective regulation of cytokine induction by adenoviral gene transfer of ikappabalpha into human macrophages: lipopolysaccharide-induced, but not zymosan-induced, proinflammatory cytokines are inhibited, but il-10 is nuclear factor-kappab independent. *J Immunol* 162(5):2939–45
- Brummer E, Kammer M, Stevens DA (2003) Regulation by granulocyte-macrophage colony-stimulating factor and/or steroids given in vivo of proinflammatory cytokine and chemokine production by bronchoalveolar macrophages in response to *Aspergillus conidia*. *J Infect Dis* 187(4):705–709. <https://doi.org/10.1086/368383>

- Carson W, Lindemann M, Baiocchi R, Linett M, Tan J, Chou C, Narula S, Caligiuri M (1995) The functional characterization of interleukin-10 receptor expression on human natural killer cells. *Blood* 85(12):3577–85
- Cassatella M (1995) The production of cytokines by polymorphonuclear neutrophils. *Immunol Today* 16(1):21–6. [https://doi.org/10.1016/0167-5699\(95\)80066-2](https://doi.org/10.1016/0167-5699(95)80066-2)
- Castell JV, Geiger T, Gross V, Andus T, Walter E, Hirano T, Kishimoto T, Heinrich PC (1988) Plasma clearance, organ distribution and target cells of interleukin-6/hepatocyte-stimulating factor in the rat. *Eur J Biochem* 177(2):357–361. <https://doi.org/10.1111/j.1432-1033.1988.tb14383.x>
- Castiglione F, Duca K, Jarrah A, Laubenbacher R, Hochberg D, Thorley-Lawson D (2007) Simulating Epstein-Barr virus infection with C-ImmSim. *Bioinformatics* 23(11):1371–1377. <https://doi.org/10.1093/bioinformatics/btm044>
- Celio GFDL, Xiao YQ, Shyra JG, Donna LB, William PS, Peter MH (2006) Apoptotic cells, through transforming growth factor- β , coordinately induce anti-inflammatory and suppress pro-inflammatory eicosanoid and no synthesis in murine macrophages. *J Biol Chem* 281:38376. <https://doi.org/10.1074/jbc.M605146200>
- Chai L, Netea M, Sugui J, Vonk A, van de Sande W, Warris A, Kwon-Chung K, Kullberg B (2010) *Aspergillus fumigatus* conidial melanin modulates host cytokine response. *Immunobiology* 215(11):915–920. <https://doi.org/10.1016/j.imbio.2009.10.002>
- Chang MJ, Chow LC, Chang WS (1991) Improved alternating-direction implicit method for solving transient three-dimensional heat diffusion problems. *Numer Heat Transf Part B Fundam* 19(1):69–84. <https://doi.org/10.1080/10407799108944957>
- Ciesielski C, Andreasko E, Foxwell B, Feldmann M (2002) Tnfa-induced macrophage chemokine secretion is more dependent on nf-kb expression than lipopolysaccharides-induced macrophage chemokine secretion. *Eur J Immunol* 32(7):2037–2045. [https://doi.org/10.1002/1521-4141\(200207\)32:7<2037::AID-IMMU2037>3.0.CO;2-I](https://doi.org/10.1002/1521-4141(200207)32:7<2037::AID-IMMU2037>3.0.CO;2-I)
- Čulić O, Eraković V, Čepelak I, Barišić K, Brajša K, Ferenčić Željko, Galović R, Glojnaric I, Manojlović Z, Munić V, Novak-Mirčetić R, Pavičić-Beljak V, Sučić M, Veljača M, Žanić-Grubišić T, Parnham MJ (2002) Azithromycin modulates neutrophil function and circulating inflammatory mediators in healthy human subjects. *Eur J Pharmacol* 450(3):277–289. [https://doi.org/10.1016/S0014-2999\(02\)02042-3](https://doi.org/10.1016/S0014-2999(02)02042-3)
- Dellière S, Dudoignon E, Fodil S, Voicu S, Collet M, Ouilic P-A, Salmona M, Dépret F, Ghelfenstein-Ferreira T, Plaud B, Chousterman B, Bretagne S, Azoulay E, Mebazaa A, Megarbane B, Alanio A (2021) Risk factors associated with covid-19-associated pulmonary aspergillosis in icu patients: a French multicentric retrospective cohort. *Clin Microbiol Infect* 27(5):790–17905. <https://doi.org/10.1016/j.cmi.2020.12.005>
- Ding A, Sanchez E, Srimal S, Nathan C (1989) Macrophages rapidly internalize their tumor necrosis factor receptors in response to bacterial lipopolysaccharide. *J Biol Chem* 264(7):3924–9
- Ding Z, Li M, Sun F, Xi P, Sun L, Zhang L, Jiang Z (2015) Mitogen-activated protein kinases are associated with the regulation of physiological traits and virulence in *Fusarium oxysporum* f. sp. *cubense*. *PLoS ONE* 10(4):0122634. <https://doi.org/10.1371/journal.pone.0122634>
- Dzhuraev G, Rodriguez-Castillo J, Ruiz-Camp J, Salwig I, Szibor M, Vadasz I, Herold S, Braun T, Ahlbrecht K, Atzberger A, Muhlfeld C, Seeger W, Morty R (2019) Estimation of absolute number of alveolar epithelial type 2 cells in mouse lungs: a comparison between stereology and flow cytometry. *J Microsc* 275:36–50. <https://doi.org/10.1111/jmi.12800>
- Ergun M, Brüggemann RJM, Alanio A, Dellière S, van Arkel A, Bentvelsen RG, Rijpstra T, van der Sar-van der Brugge S, Lagrou K, Janssen NAF, Buil JB, van Dijk K, Melchers WJG, Reijers MHE, Schouten JA, Wauters J, Cordey A, SoniS White PL, van de Veerdonk FL, Verweij PE, Hanson KE (2021) *Aspergillus* test profiles and mortality in critically ill covid-19 patients. *J Clin Microbiol* 59(12):01229–21. <https://doi.org/10.1128/JCM.01229-21>
- Escobar N, Ordóñez SR, Wösten HAB, Haas P-JA, de Cock H, Haagsman HP (2016) Hide, keep quiet, and keep low: properties that make *Aspergillus fumigatus* a successful lung pathogen. *Front Microbiol*. <https://doi.org/10.3389/fmicb.2016.00438>
- Fadok VA, Bratton DL, Konowal A, Freed PW, Westcott JY, Henson PM (1998) Macrophages that have ingested apoptotic cells in vitro inhibit proinflammatory cytokine production through autocrine/paracrine mechanisms involving tgf-beta, pge2, and paf. *J Clin Investig*. <https://doi.org/10.1172/JCI1112>

- Fadok VA, Bratton DL, Guthrie L, Henson PM (2001) Differential effects of apoptotic versus lysed cells on macrophage production of cytokines: role of proteases. *J Immunol* 166(11):6847–6854. <https://doi.org/10.4049/jimmunol.166.11.6847>
- Fujishima S, Hoffman AR, Kim VuKJT, Zheng H, Daniel D, Kim WY, Wallace EF, Larrick JW, Raffin TA (1993) Regulation of neutrophil interleukin 8 gene expression and protein secretion by lps, tnf- α , and il-1 β . *J Cell Physiol* 154:478–485. <https://doi.org/10.1002/jcp.1041540305>
- Gago S, Overton N, Ben Ghaziz N, Novak-Frazer L, Read N, Denning D, Bowyer P (2018) Lung colonization by *Aspergillus fumigatus* is controlled by znf77. *Nat Commun*. <https://doi.org/10.1038/s41467-018-06148-7>
- Gazendam RP, van Hamme JL, Tool AT, Hoogenboezem M, van den Berg JM, Prins JM, Vitkov L, van de Veerdonk FL, van den Berg TK, Roos D, Kuijpers TW (2016a) Human neutrophils use different mechanisms to kill *Aspergillus fumigatus* conidia and hyphae: evidence from phagocyte defects. *J Immunol* 196(3):1272–1283. <https://doi.org/10.4049/jimmunol.1501811>
- Gazendam R, van de Geer A, van Hamme J, Tool A, van Rees D, Aarts C, van den Biggelaar M, van Alphen F, Verkuijlen P, Meijer A, Janssen H, Roos D, van den Berg T, Kuijpers T (2016b) Impaired killing of *Candida albicans* by granulocytes mobilized for transfusion purposes: a role for granule components. *Haematologica* 101(5):587–96. <https://doi.org/10.3324/haematol.2015.136630>
- Gersuk GM, Underhill DM, Zhu L, Marr KA (2006) Dectin-1 and tlr5 permit macrophages to distinguish between different *Aspergillus fumigatus* cellular states. *J Immunol* 176(6):3717–3724. <https://doi.org/10.4049/jimmunol.176.6.3717>
- Goncalves SM, Lagrou K, Rodrigues CS, Campos CF, Bernal-Martinez L, Rodrigues F, Silvestre R, Alcazar-Fuoli L, Maertens JA, Cunha C, Carvalho A (2017) Evaluation of bronchoalveolar lavage fluid cytokines as biomarkers for invasive pulmonary aspergillosis in at-risk patients. *Front Microbiol* 8:2362. <https://doi.org/10.3389/fmicb.2017.02362>
- Gong D, Farley K, White M, Hartshorn KL, Benarafa C, Remold-O'Donnell E (2011) Critical role of SerpinB1 in regulating inflammatory responses in pulmonary influenza infection. *J Infect Dis* 204(4):592–600. <https://doi.org/10.1093/infdis/jir352>
- Goodhill GJ (1997) Diffusion in axon guidance. *Eur J Neurosci* 9:1414–1421. <https://doi.org/10.1111/j.1460-9568.1997.tb01496.x>
- Goodhill G (1998) Mathematical guidance for axons. *Trends Neurosci* 21(6):226–231. [https://doi.org/10.1016/s0166-2236\(97\)01203-4](https://doi.org/10.1016/s0166-2236(97)01203-4)
- Grunwell J, Giacalone V, Stephenson S, Margaroli C, Dobosh B, Brown M, Fitzpatrick A, Tirouvanziam R (2019) Neutrophil dysfunction in the airways of children with acute respiratory failure due to lower respiratory tract viral and bacterial coinfections. *Sci Rep* 9:2874. <https://doi.org/10.1038/s41598-019-39726-w>
- Ho AS, Liu Y, Khan TA, Hsu DH, Bazan JF, Moore KW (1993) A receptor for interleukin 10 is related to interferon receptors. *Proc Natl Acad Sci* 90(23):11267–11271. <https://doi.org/10.1073/pnas.90.23.11267>
- Hohl T, Van Epps H, Rivera A, Morgan L, Chen P et al (2005) *Aspergillus fumigatus* triggers inflammatory responses by stage-specific b-glucan display. *PLoS Pathog* 1(3):30. <https://doi.org/10.1371/journal.ppat.0010030>
- Hohmann H, Remy R, Brockhaus M, van Loon A (1989) Two different cell types have different major receptors for human tumor necrosis factor (tnf alpha). *J Biol Chem* 264(25):14927–34
- Hsu JL, Manouvakhova OV, Clemons KV, Inayathullah M, Tu AB, Sobel RA, Tian A, Nazik H, Pothineni VR, Pasupneti S et al (2018) Microhemorrhage-associated tissue iron enhances the risk for *Aspergillus fumigatus* invasion in a mouse model of airway transplantation. *Sci Transl Med* 10(429):2616
- Huhn RD, Radwanski E, Gallo J, Affrime MB, Sabo R, Gonyo G, Monge A, Cutler DL (1997) Pharmacodynamics of subcutaneous recombinant human interleukin-10 in healthy volunteers. *Clin Pharmacol Therap* 62(2):171–180. [https://doi.org/10.1016/S0009-9236\(97\)90065-5](https://doi.org/10.1016/S0009-9236(97)90065-5)
- Jablonski H, Rekasi H, Jager M (2016) The influence of calcitonin gene-related peptide on markers of bone metabolism in mg-63 osteoblast-like cells co-cultured with thp-1 macrophage-like cells under virtually osteolytic conditions. *BMC Musculoskelet Disord*. <https://doi.org/10.1186/s12891-016-1044-5>
- Johnson JW, Lebreton JM (2004) History and use of relative importance indices in organizational research. *Organ Res Methods* 7(3):238–257. <https://doi.org/10.1177/1094428104266510>
- Kalter VG, Brody AR (1991) Receptors for transforming growth factor- β (tgf- β) on rat lung fibroblasts have higher affinity for tgf- β 1 than for tgf- β 2. *Am J Respir Cell Mol Biol* 4(5):397–407. <https://doi.org/10.1165/ajrcmb/4.5.397>

- Kariyawasam RM, Dingle TC, Kula BE, Sligl WI, Schwartz IS (2021) Covid-19 associated pulmonary Aspergillosis: systematic review and patient-level meta-analysis. medRxiv
- Katsuo K, Bo-Ram O (2014) Optofluidic cellular immunofunctional analysis by localized surface Plasmon resonance. In: Proceedings of SPIE 9166, Biosensing and Nanomedicine VII, 91660R. <https://doi.org/10.1117/12.2062244>
- Khandoga A, Khandoga A, Reichel C, Bihari P, Rehberg M et al (2009) In vivo imaging and quantitative analysis of leukocyte directional migration and polarization in inflamed tissue. PLoS ONE 4(3):4693. <https://doi.org/10.1371/journal.pone.0004693>
- Kuribayashi T (2018) Elimination half-lives of interleukin-6 and cytokine-induced neutrophil chemoattractant-1 synthesized in response to inflammatory stimulation in rats. Lab Anim Res 34:80–83. <https://doi.org/10.5625/lar.2018.34.2.80>
- Lai C-C, Yu W-L (2021) Covid-19 associated with pulmonary aspergillosis: a literature review. J Microbiol Immunol Infect 54(1):46–53. <https://doi.org/10.1016/j.jmii.2020.09.004>
- Latge J-P (1999) *Aspergillus fumigatus* and aspergillosis. Clin Microbiol Rev 12(2):310–350. <https://doi.org/10.1128/CMR.12.2.310>
- Liu Y, Wei S, Ho A, de Waal MR, Moore K (1994) Expression cloning and characterization of a human il-10 receptor. J Immunol 152(4):1821–9
- Loeffler J, Haddad Z, Bonin M, Romeike N, Mezger M, Schumacher U, Kapp M, Gebhardt F, Grigoleit G-U, Stevanović S, Einsele H, Hebart H (2009) Interaction analyses of human monocytes co-cultured with different forms of *Aspergillus fumigatus*. J Med Microbiol 58(1):49–58. <https://doi.org/10.1099/jmm.0.003293-0>
- Lord PC, Wilmoth LM, Mizel SB, McCall CE (1991) Expression of interleukin-1 alpha and beta genes by human blood polymorphonuclear leukocytes. J Clin Invest 87(4):1312–1321. <https://doi.org/10.1172/JCI115134>
- Mackel JJ, Steele C (2019) Host defense mechanisms against *Aspergillus fumigatus* lung colonization and invasion. Curr Opin Microbiol 52:14–19. <https://doi.org/10.1016/j.mib.2019.04.003>
- Maheshwari R (2005) Fungi experimental methods in biology. CRC Press, Cambridge
- Marika K, Elmer B, Davidm AS (2002) Regulation of bronchoalveolar macrophage proinflammatory cytokine production by dexamethasone and granulocyte-macrophage colony-stimulating factor after stimulation by *Aspergillus conidia* or lipopolysaccharide. Cytokine 19(1):14–20. <https://doi.org/10.1006/cyto.2002.1049>
- Massague J, Like B (1985) Cellular receptors for type beta transforming growth factor: ligand binding and affinity labeling in human and rodent cell lines. J Biol Chem 260(5):2636–45
- Meletiadiis J, Meis JFGM, Mouton JW, Verweij PE (2001) Analysis of growth characteristics of filamentous fungi in different nutrient media. J Clin Microbiol 39(2):478–484. <https://doi.org/10.1128/JCM.39.2.478-484.2001>
- Michels K, Solomon AL, Scindia Y, Sordo Vieira L, Goddard Y, Whitten S, Vaulont S, Burdick MD, Atkinson C, Laubenbacher R et al (2022) *Aspergillus* utilizes extracellular heme as an iron source during invasive pneumonia, driving infection severity. J Infect Dis 225(10):1811–1821
- Mihai GN, Warris A, Jos WMVdM, Matthew JF, Trees JGV-J, Liesbeth EHJ, Andresen T, Paul EV, Bart JK (2003) *Aspergillus fumigatus* evades immune recognition during germination through loss of toll-like receptor-4-mediated signal transduction. J Infect Dis 188(2):320–326. <https://doi.org/10.1086/376456>
- Mitaka H, Kuno T, Takagi H, Patrawalla P (2021) Incidence and mortality of covid-19-associated pulmonary aspergillosis: a systematic review and meta-analysis. Mycoses 64(9):993–1001. <https://doi.org/10.1111/myc.13292>
- Okazaki M, Adachi Y, Ohno N, Yadomae T (1995) Structure–activity relationship of (1 → 3)-beta-d-glucans in the induction of cytokine production from macrophages, in vitro. Biol Pharm Bull 18(10):1320–7. <https://doi.org/10.1248/bpb.18.1320>
- Oliver J, Bland L, Oettinger C, Arduino M, McAllister S, Aguero S, Favero M (1993) Cytokine kinetics in an in vitro whole blood model following an endotoxin challenge. Lymphokine Cytokine Res 12(2):115–120
- Oremland M, Michels K, Bettina A, Lawrence C, Mehrad B, Laubenbacher R (2016) A computational model of invasive aspergillosis in the lung and the role of iron. BMC Syst Biol. <https://doi.org/10.1186/s12918-016-0275-2>
- Palmberg L, Larsson B, Malmberg P, Larsson K (1998) Induction of il-8 production in human alveolar macrophages and human bronchial epithelial cells in vitro by swine dust. Thorax 53(4):260–4. <https://doi.org/10.1136/thx.53.4.260>

- Pappas P et al (2010) Invasive fungal infections among organ transplant recipients: results of the transplant-associated infection surveillance network (transnet). *Clin Infect Dis* 50:1101–11
- Patel A, Zhang Y, Fullerton J, Boelen L, Rongvaux A, Maini A, Bigley V, Flavell R, Gilroy D, Asquith B, Macallan D, Yona S (2017) The fate and lifespan of human monocyte subsets in steady state and systemic inflammation. *J Exp Med*. <https://doi.org/10.1084/jem.20170355>
- Pollmächer J, Figge MT (2014) Agent-based model of human alveoli predicts chemotactic signaling by epithelial cells during early *Aspergillus fumigatus* infection. *PLoS ONE* 9(10):111630
- Renshaw H, Vargas-Muñiz J, Juvvadi P, Richards A, Waitt G, Soderblom E, Moseley M, Steinbach W (2018) The tail domain of the *Aspergillus fumigatus* class v myosin myoe orchestrates septal localization and hyphal growth. *J Cell Sci* 131(3):205955. <https://doi.org/10.1242/jcs.205955>
- Ribeiro H, Maioli T, de Freitas L, Tieri P, Castiglione F (2017) Modeling immune response to *Leishmania* species indicates adenosine as an important inhibitor of th-cell activation. *Front Cell Infect Microbiol*. <https://doi.org/10.3389/fcimb.2017.00309>
- Ribeiro HAL, Vieira LS, Scindia Y, Adhikari B, Wheeler M, Knapp A, Schroeder W, Mehrad B, Laubenschacher R (2022) Multi-scale mechanistic modelling of the host defence in invasive aspergillosis reveals leucocyte activation and iron acquisition as drivers of infection outcome. *J R Soc Interface* 19(189):20210806. <https://doi.org/10.1098/rsif.2021.0806>
- Riquelme M, Bartnicki-Garcia S (2004) Key differences between lateral and apical branching in hyphae of *Neurospora crassa*. *Fungal Genet Biol* 41(9):842–851. <https://doi.org/10.1016/j.fgb.2004.04.006>
- Rodrigues AG, Araujo R, Pina-Vaz C (2005) Human albumin promotes germination, hyphal growth and antifungal resistance by *Aspergillus fumigatus*. *Med Mycol* 43(8):711–717. <https://doi.org/10.1080/13693780500129814>
- Roilides E, Holmes A, Blake C, Venzon D, Pizzo P, Walsh T (1994) Antifungal activity of elutriated human monocytes against *Aspergillus fumigatus* hyphae: enhancement by granulocyte-macrophage colony-stimulating factor and interferon-gamma. *J Infect Dis* 170(4):894–9. <https://doi.org/10.1093/infdis/170.4.894>
- Roilides E, Sein T, Holmes A, Chanock S, Blake C, Pizzo P, Walsh T (1995) Effects of macrophage colony-stimulating factor on antifungal activity of mononuclear phagocytes against *Aspergillus fumigatus*. *J Infect Dis* 172(4):1028–1034. <https://doi.org/10.1093/infdis/172.4.1028>
- Roilides E, Dimitriadou-Georgiadou A, Sein T, Kadiltsoğlu I, Walsh T (1998) Tumor necrosis factor alpha enhances antifungal activities of polymorphonuclear and mononuclear phagocytes against *Aspergillus fumigatus*. *Infect Immun* 66(12):5999–6003. <https://doi.org/10.1128/IAI.66.12.5999-6003.1998>
- Sai J, Fan G-H, Wang D, Richmond A (2004) The c-terminal domain Ilk1 motif of cxcr2 is required for ligand-mediated polarization of early signals during chemotaxis. *J Cell Sci* 117(23):5489–5496. <https://doi.org/10.1242/jcs.01398>
- Samson M, LaRosa G, Libert F, Paindavoine P, Detheux M, Vassart G, Parmentier M (1997) The second extracellular loop of ccr5 is the major determinant of ligand specificity. *J Biol Chem* 272(40):24934–24941. <https://doi.org/10.1074/jbc.272.40.24934>
- Schall T, Lewis M, Koller K, Lee A, Rice G, Wong G, Gatanaga T, Granger G, Lentz R, Raab H et al (1990) Molecular cloning and expression of a receptor for human tumor necrosis factor. *Cell* 61(2):361–70. [https://doi.org/10.1016/0092-8674\(90\)90816-w](https://doi.org/10.1016/0092-8674(90)90816-w)
- Segrelles-Calvo G, Araújo GRS, Llopis-Pastor E, Carrillo J, Hernández-Hernández M, Rey L, Rodríguez Melean N, Escribano I, Antón E, Zamarro C, García-Salmónes M, Frases S (2021) Prevalence of opportunistic invasive aspergillosis in covid-19 patients with severe pneumonia. *Mycoses* 64(2):144–151. <https://doi.org/10.1111/myc.13219>
- Sharif O, Bolshakov VN, Raines S et al (2007) Transcriptional profiling of the lps induced nf- κ b response in macrophages. *BMC Immunol*. <https://doi.org/10.1186/1471-2172-8-1>
- Simitsopoulou M, Roilides E, Likartsis C, Ioannidis J, Orfanou A, Paliogianni F, Walsh TJ (2007) Expression of immunomodulatory genes in human monocytes induced by voriconazole in the presence of *Aspergillus fumigatus*. *Antimicrob Agents Chemother* 51(3):1048–1054. <https://doi.org/10.1128/AAC.01095-06>
- Stauber G, Aiyer R, Aggarwal B (1988) Human tumor necrosis factor-alpha receptor: purification by immunoaffinity chromatography and initial characterization. *J Biol Chem* 263(35):19098–104
- Steele C, Rapaka R, Metz A, Pop S, Williams D et al (2005) The beta-glucan receptor dectin-1 recognizes specific morphologies of *Aspergillus fumigatus*. *PLoS Pathog* 1(4):42. <https://doi.org/10.1371/journal.ppat.0010042>

- Stites S, Nelson M, Wesselius L (1995) Transferrin concentrations in serum and lower respiratory tract fluid of mechanically ventilated patients with copd or ards. *Dis Chest* 107(6):1681–1685. <https://doi.org/10.1378/chest.107.6.1681>
- Tak T, Tesselaar K, Pillay J, Borghans J, Koenderman L (2013) What's your age again? determination of human neutrophil half-lives revisited. *J Leukoc Biol* 94(4):595–601. <https://doi.org/10.1189/jlb.1112571>
- Tan J, Indelicato S, Narula S, Zavodny P, Chou C (1993) Characterization of interleukin-10 receptors on human and mouse cells. *J Biol Chem* 268(28):21053–21059
- Tappe B, Lauruschkat CD, Strobel L, García JP, Kurzai O, Rebhan S, Kraus S, Pfeuffer-Jovic E, Bussemmer L, Possler L et al (2022) Covid-19 patients share common, corticosteroid-independent features of impaired host immunity to pathogenic molds. *Front Immunol*. <https://doi.org/10.3389/fimmu.2022.954985>
- Taylor P, Tsoni S, Willment J et al (2007) Dectin-1 is required for β -glucan recognition and control of fungal infection. *Nat Immunol* 8:31–38. <https://doi.org/10.1038/ni1408>
- Taylor P, Roy S, Leal S et al (2014) Activation of neutrophils by autocrine il-17a-il-17rc interactions during fungal infection is regulated by il-6, il-23, roryt and dectin-2. *Nat Immunol* 15:3007–3017. <https://doi.org/10.1038/ni.2797>
- Thorley AJ, Ford PA, Giembycz MA, Goldstraw P, Young A, Tetley TD (2007) Differential regulation of cytokine release and leukocyte migration by lipopolysaccharide-stimulated primary human lung alveolar type ii epithelial cells and macrophages. *J Immunol* 178(1):463–473. <https://doi.org/10.4049/jimmunol.178.1.463>
- Toft A, Falahati A, Steensberg A (2011) Source and kinetics of interleukin-6 in humans during exercise demonstrated by a minimally invasive model. *Eur J Appl Physiol* 111:1351–1359. <https://doi.org/10.1007/s00421-010-1755-5>
- Trinci APJ (1973) The hyphal growth unit of wild type and spreading colonial mutants of *Neurospora crassa*. *Archiv Mikrobiol* 91:127–136. <https://doi.org/10.1007/BF00424756>
- Tsujimoto M, Vilcek J (1987) Tumor necrosis factor-induced downregulation of its receptors in HeLa cells. *J Biochem* 102(6):1571–1577. <https://doi.org/10.1093/oxfordjournals.jbchem.a122206>
- Tsujimoto M, Yip YK, Vilcek J (1985) Tumor necrosis factor: specific binding and internalization in sensitive and resistant cells. *Proc Natl Acad Sci* 82(22):7626–7630. <https://doi.org/10.1073/pnas.82.22.7626>
- Verweij P, Gangneux J, Bassetti M, Brüggemann R, Cornely O, Koehler P, Lass-Flörl C, van de Veerdonk F, Chakrabarti A, Hoenigl M (2020) Diagnosing covid-19-associated pulmonary aspergillosis. *Lancet Microbe*. 1(2):53–55. [https://doi.org/10.1016/S2666-5247\(20\)30027-6](https://doi.org/10.1016/S2666-5247(20)30027-6)
- Wakefield L, Smith D, Masui T, Harris C, Sporn M (1987) Distribution and modulation of the cellular receptor for transforming growth factor-beta. *J Cell Biol* 105(2):965–75. <https://doi.org/10.1083/jcb.105.2.965>
- Wakefield L, Winokur T, Hollands R, Christopherson K, Levinson A, Sporn M (1990) Recombinant latent transforming growth factor beta 1 has a longer plasma half-life in rats than active transforming growth factor beta 1, and a different tissue distribution. *J Clin Invest* 86(6):1976–1984. <https://doi.org/10.1172/JCI114932>
- Warris A, Netea M, Verweij P, Gaustad P, Kullberg B, Weemaes C, Abrahamsen T (2005) Cytokine responses and regulation of interferon-gamma release by human mononuclear cells to *Aspergillus fumigatus* and other filamentous fungi. *Med Mycol* 43(7):613–21. <https://doi.org/10.1080/13693780500088333>
- Werner JL, Metz AE, Horn D, Schoeb TR, Hewitt MM, Schwiebert LM, Faro-Trindade I, Brown GD, Steele C (2009) Requisite role for the dectin-1 b-glucan receptor in pulmonary defense against *Aspergillus fumigatus*. *J Immunol* 182(8):4938–4946. <https://doi.org/10.4049/jimmunol.0804250>
- Xing L, Remick D (2003) Relative cytokine and cytokine inhibitor production by mononuclear cells and neutrophils. *Shock* 20(1):10–6. <https://doi.org/10.1097/01.shk.0000065704.84144.a4>
- Xu J, Yang X, Lv Z, Zhou T, Liu H, Zou X, Cao F, Zhang L, Liu B, Chen W et al (2021) Risk factors for invasive aspergillosis in patients admitted to the intensive care unit with coronavirus disease 2019: a multicenter retrospective study. *Front Med* 8:753659
- Zahn G, Greischel A (1989) Pharmacokinetics of tumor necrosis factor alpha after intravenous administration in rats: dose dependence and influence of tumor necrosis factor beta. *Arzneimittelforschung* 39(9):1180–1182
- Zarembek K, Sugui J, Chang Y, Kwon-Chung K, Gallin J (2007) Human polymorphonuclear leukocytes inhibit *Aspergillus fumigatus* conidial growth by lactoferrin-mediated iron depletion. *J Immunol* 178(10):6367–6373. <https://doi.org/10.4049/jimmunol.178.10.6367>

Publisher's Note Springer Nature remains neutral with regard to jurisdictional claims in published maps and institutional affiliations.

Springer Nature or its licensor (e.g. a society or other partner) holds exclusive rights to this article under a publishing agreement with the author(s) or other rightsholder(s); author self-archiving of the accepted manuscript version of this article is solely governed by the terms of such publishing agreement and applicable law.